IOPscience iopscience.iop.org

Home Search Collections Journals About Contact us My IOPscience

Quantitative schlieren diagnostics for the determination of ambient species density, gas temperature and calorimetric power of cold atmospheric plasma jets

This content has been downloaded from IOPscience. Please scroll down to see the full text.

2015 J. Phys. D: Appl. Phys. 48 175202

(http://iopscience.iop.org/0022-3727/48/17/175202)

View the table of contents for this issue, or go to the journal homepage for more

Download details:

IP Address: 149.150.51.237
This content was downloaded on 04/04/2015 at 14:25

Please note that terms and conditions apply.

IOP Publishing Journal of Physics D: Applied Physics
J. Phys. D: Appl. Phys. **48** (2015) 175202 (9pp) doi:10.1088/0022-3727/48/17/175202

Quantitative schlieren diagnostics for the determination of ambient species density, gas temperature and calorimetric power of cold atmospheric plasma jets

A Schmidt-Bleker, S Reuter and K-D Weltmann

INP Greifswald / ZIK plasmatis, Felix-Hausdorff-Str. 2, 17489 Greifswald, Germany

E-mail: ansgar.schmidt-bleker@inp-greifswald.de and stephan.reuter@inp-greifswald.de

Received 18 December 2014, revised 27 February 2015
Accepted for publication 9 March 2015
Published 31 March 2015

Abstract

A measurement and evaluation technique for performing quantitative Schlieren diagnostics on an argon-operated cold atmospheric plasma jet is presented. Combined with computational fluid dynamics simulations, the method not only yields the temporally averaged ambient air density and temperature in the effluent of the fully turbulent jet, but also allows for an estimation of the calorimetric power deposited by the plasma.

The change of the refractive index due to mixing of argon and air is in the same range as caused by the temperature increase of less than 35 K in the effluent of the plasma jet. The Schlieren contrast therefore needs to be corrected for the contribution from ambient air diffusion. The Schlieren system can be calibrated accurately using the signal obtained from the argon flow when the plasma is turned off. The temperature measured in this way is compared to the value obtained using a fibre-optics temperature probe and shows excellent agreement. By fitting a heat source in a fluid dynamics simulation to match the measured temperature field, the calorimetric power deposited by the plasma jet can be estimated as 1.1 W.

Keywords: plasma jet, schlieren, gas temperature, gas density, CFD, calorimetry

(Some figures may appear in colour only in the online journal)

1. Introduction

Knowledge about ambient air diffusion and temperature is a vital information for atmospheric pressure plasma sources. Schlieren imaging is a common technique for the visualization of fluid flows and several textbooks give good introductions to the topic [1–4]. Cold atmospheric plasma (CAP) jets are employed as tools in the novel field of plasma medicine [5–8]. For both the biomedical application and for understanding basic chemical mechanisms in low temperature plasmas, a detailed knowledge about the gas temperature and ambient air diffusion into the active plasma zone is crucial. Schlieren imaging has been used to qualitatively study the interaction of the plasma and gas flow in such devices for various geometries and feed gases [9–13]. For plasma sources operated at higher temperatures also quantitative Schlieren [14] or similar techniques including laser Schlieren deflectometry [15] and quantitative shadowgraphy [16] have been used to determine the gas temperature in the respective plasma devices. However, to the best of the authors knowledge quantitative Schlieren diagnostics have not yet been used for the determination of air densities and gas temperature in CAP jets operating close to room temperature.

With the quantitative Schlieren measurement and evaluation technique presented in this work the temporally averaged argon and accordingly air density as well as the averaged temperature of the fully turbulent CAP jet kinpen Sci is measured by Schlieren imaging. Additionally the calorimetric power deposition is estimated by combining the Schlieren measurements with computational fluid dynamics (CFD) simulations. This

 © 2015 IOP Publishing Ltd Printed in the UK

is challenging as the gas temperature rises by less than 35 K when the plasma is turned on and consequently the change in refractive index due to gas heating lies in the same range as the change due to gas mixing of argon and air. Obtaining both the ambient air density and the gas temperature requires two subsequent measurements with plasma turned off and turned on. In order to be accurate, the method requires that the diffusion process is not significantly affected when the plasma is turned on. Previously the ambient species diffusion was studied using a VUV absorption method combined with an analytical model [17, 18] and molecular beam mass spectrometry [19] and it was found, that the ambient species diffusion into the effluent of the CAP jet is not significantly changed when the plasma is turned on at an argon flux of 3 slm. However, both measurements were performed with the jet not operating in open air, but impinging upon a plate. Several groups have shown, that the plasma can significantly influence the fluid dynamics and a transition of flow regime from laminar to turbulent (or vice versa) can occur when the plasma is switched on [10, 12, 20–22]. This is attributed to electrohydrodynamic forces or temperature effects. In a previous study on the kinpen using planar laser induced fluorescence (PLIF) spectroscopy on OH as tracer molecule (with plasma turned on) as well as PLIF on acetone (with plasma turned off) it was found that while a laminar to turbulent transition does occur at lower feed gas flow rates (1 slm) when the jet is turned on, the flow remains turbulent at a flow rate of 3 slm [23]. The CAP jet is operated in the turbulent regime at an argon flow rate of 3 slm (standard liter per minute) corresponding to a Reynolds number of Re = 2980. Besides quantitative Schlieren diagnostics, the temperature is also measured using a non-metallic fiber-optics probe. Although probe measurements are likely to disturb the plasma and the temperature measurement, very good agreement between both techniques was found. Computational fluid dynamics (CFD) simulations are performed and compared to the Schlieren results. While in the simulation the plasma is merely considered as a heat source, the agreement between the measured and simulated flow fields and temperature distributions in the far-field is very good. The heat source employed in the simulation is consequently used to estimate the calorimetric power in the downstream region of the jet.

2. Methods

2.1. Plasma jet

The plasma jet kinpen Sci previously introduced in [19] is used. As feed gas dry argon at a mass flow rate of 3 slm is used. The jet features a powered inner needle electrode that is mounted in the center of a capillary with radius $r_0 = 0.8$ mm and a grounded outer electrode that can be seen in the image of the jet in figure 1. The inner electrode is driven at a frequency of ∼0.9 MHz and a peak-to-peak Voltage of 2.1 kV. The visible plasma effluent measures about 12 mm in length.

2.2. Schlieren diagnostics

2.2.1. Setup. In figure 2 the experimental setup for the Schlieren and probe measurements is shown. The point light source is constructed by focusing the light from a green LED lamp (HighLED-G, Linos Photonics GmbH, Germany) on an aperture with a diameter of $d = 0.2$ mm. Between the focusing lens and and the aperture a diffusion disc is placed in order to achieve an homogeneous lighting in the test region. The aperture is placed in the focal point of a best-form lens (focal length $f = 200$ mm), which creates the parallel light test region of the Schlieren system. Best form lenses are used in order to minimize spherical aberration. After passing through the test region in which the plasma jet is placed, the parallel light is again focused by another lens ($f = 200$ mm) on the knife edge. The knife edge is adjusted so that the detected intensity signal is reduced to approximately 42% of the signal without knife edge. The Schlieren signal is imaged using a simple 8 bit USB camera (DCC1545M, Thorlabs, USA). In front of the camera a dielectric filter with a transmission wavelength of 550 nm at a full width at half maximum of 10 nm is used. The combination of a green light source and this filter is chosen as the jet does not emit any light in this wavelength region. As the light intensity from the point source is not very high due to the small aperture, any light emitted by the jet makes the measurement impossible. It is noted, that a subsequent subtraction of the light emitted by the plasma jet is difficult, as the emission is not perfectly constant in time. For probe measurements of the gas temperature, a non-metallic fiber-optics probe mounted on a three-axis linear table is used. The device determines the temperature by spectroscopically measuring the band gap of a GaAs crystal which is deposited at the tip of the optical fiber (FOTEMP1-OEM and TS3, Optocon AG, Germany).

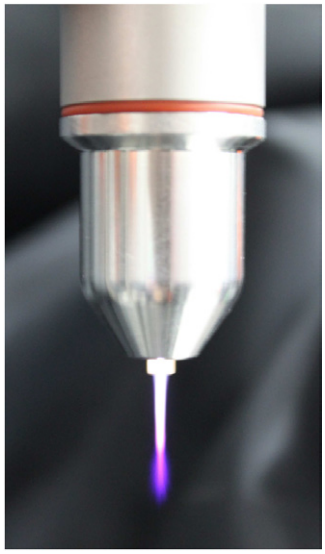

Figure 1. Image of the argon-operated plasma jet kinpen Sci.

2.2.2. Theory. The refractive index of a gaseous medium depends on the molecular composition, its density or pressure and the wavelength. The well-known Lorenz–Lorentz (also termed Clausius–Mossotti) equation

$$\frac{n^2-1}{n^2+2} = \frac{4\pi}{3} N \sum_i x_i \alpha_i \qquad (1)$$

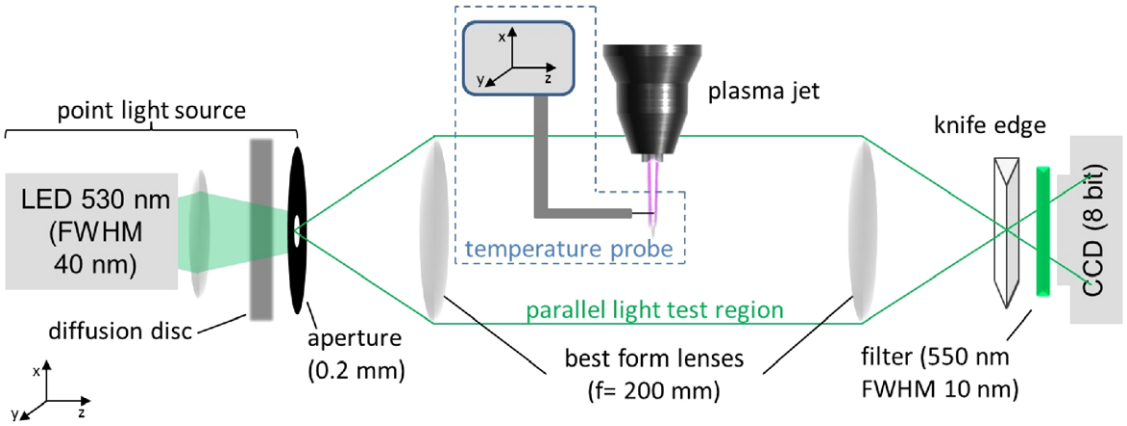

Figure 2. Experimental setup.

relates the refractive index n of a medium at a given wavelength to the mean polarizability α_i of species i at the molar fraction x_i and particle density N. For gases the deviation from the refractive index in vacuum $n - 1 = \epsilon \ll 1$ is very small. Expanding (1) to first order in ϵ yields the Gladstone–Dale relation

$$\epsilon = N/N_r \sum_i \epsilon_{r,i} x_i = \frac{pT_r}{Tp_r} \sum_i \epsilon_{r,i} x_i., \tag{2}$$

where $1 + \epsilon_{r_i}$ denotes a reference index of refraction for species i at density N_r. In equation (2) the density can be replaced by the pressure p and temperature T using the ideal gas law. Note that in the literature equation (2) is often formulated using mass fractions instead of molar fractions. A Schlieren measurement of the temperature hence requires knowledge of the local gas composition, pressure and reference values $n_{r,\,i}$ for the refractive indices which can be found in the literature. The Schlieren system measures the derivative of the refractive index in y-direction (determined by the orientation of the knife edge). As the parallel light beam passes the test region in z-direction, the signal is integrated in z-direction. It can be shown (see e.g. [1]), that the intensity I measured on the detector relates to the refractive index in the test region for $\epsilon \ll 1$ via the measured contrast

$$c = \frac{I - I_k}{I_k} = S \int_{-\infty}^{\infty} \frac{\partial n}{\partial y} \,\mathrm{d}z = S \frac{\partial}{\partial y} \left(2 \int \frac{n(r) r}{\sqrt{y^2 - r^2}} \,\mathrm{d}r \right). \tag{3}$$

Here I_k is the signal measured without any Schlieren in the test region and an axisymmetric distribution of the gas causing the Schlieren signal is assumed, where the axis points in x-direction. S is the sensitivity of the Schlieren system and is determined by the geometry of the setup and can either be calculated as discussed in the appendix A or obtained from the experimental data as described in section 3. Equation (3) is the y-derivative of the Abel transform of $n(r)S$. Using Abels inversion formula, $n(r)$ can be calculated from

$$n(r) - n_0 = \frac{1}{S} \underbrace{\int_r^{\infty} \frac{c(y)\,\mathrm{d}y}{\pi \sqrt{y^2 - r^2}}}_{\hat{c}(n)}. \tag{4}$$

Note, that compared to the standard Abel inversion formula, $c(y)$ is not derived in y-direction in $\hat{c}$, as the Schlieren system already gives the y-derived quantity. In the following, we will term $\hat{c}$ as modified Abel inversion of c. Together with (2) this yields

$$n_0 + \hat{c}/S - 1 = \frac{N}{N_r} \sum_i \epsilon_{r,i} x_i. \tag{5}$$

The determination of the temperature now requires two measurements: First, the mole fraction of argon and air need to be determined. This can be achieved by measuring the contrast $c_{\mathrm{fl.}}$ when only the gas flow is turned on, but the plasma is not ignited. In a second measurement, the plasma is turned on and the respective contrast $c_{\mathrm{pl.}}$ is measured. The gas temperature in the effluent can be determined using equation (5) together with the ideal gas law:

$$T = T_0 \frac{n_0 + \hat{c}_{\mathrm{fl.}}/S - 1}{n_0 + \hat{c}_{\mathrm{pl.}}/S - 1} F \tag{6}$$

with factor

$$F = \frac{\epsilon_{\mathrm{r,air}} + x_{\mathrm{Ar,pl.}}(n_{\mathrm{Ar}} - n_{\mathrm{air}})}{\epsilon_{\mathrm{r,air}} + x_{\mathrm{Ar,fl.}}(n_{\mathrm{Ar}} - n_{\mathrm{air}})}, \tag{7}$$

where T_0 denotes the ambient gas temperature.

2.2.3. Data processing. In order to determine the contrast, the intensity I is measured for the plasma on and plasma off case and is then divided by I_0 as evident from equation (3). The relative intensities are obtained by averaging a 1280 × 1024 pixel, 1000-frame video sequence with an exposure time of 89 ms per frame. Figure 3 shows the contrast $c_{\mathrm{fl.}}$ and $c_{\mathrm{pl.}}$ obtained for both measurements.

Before a modified Abel inversion can be performed, the axis of symmetry needs to be determined. As shown in figure 4, the centerline can accurately be found by displaying only data that is close to zero. Before further processing, it is essential to turn the image so that the axis of symmetry points in vertical direction. In figure 5 the contrast along the two lateral cuts indicated in figure 3 is shown. The lateral cut at 1.5 mm shown in figure 5(*a*) demonstrates that the signal in the plasma on case is not completely symmetric in the near field. However, already at a distance of 5 mm the asymmetry vanishes. Although the data is already very smooth due to the averaging procedure,

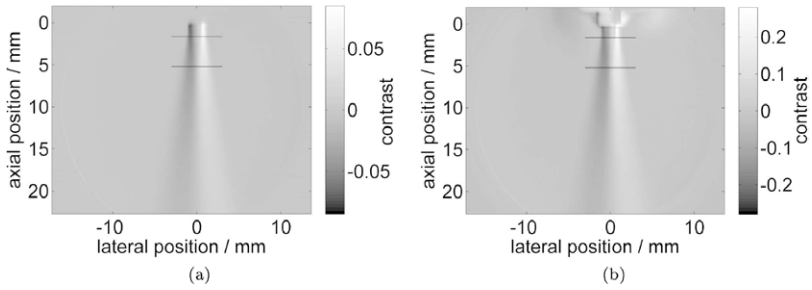

Figure 3. Schlieren contrast obtained (*a*) for an argon gas flow of 3 slm and (*b*) when plasma is turned on.

a smoothing algorithm [24] is employed to speed-up the modified Abel inversion. The data is then interpolated using piecewise cubic Hermite polynomials. The expression for $\hat{c}$ in equation (4) assumes that the data is point symmetric and hence only takes values of $c(y)$ for $y > 0$ into account. In order to use the complete measured data the values for $y < 0$ inverted in the point of origin and the contributions from $y < 0$ and $y > 0$ are then averaged, as illustrated by the dashed line in figure 5. Now the Integral $\hat{c}$ is calculated for each line in the region of interest. As noise should not be integrated in the modified Abel-Inversion, an upper integration limit is set for each row of the image, as indicated by the dashed line in figure 4.

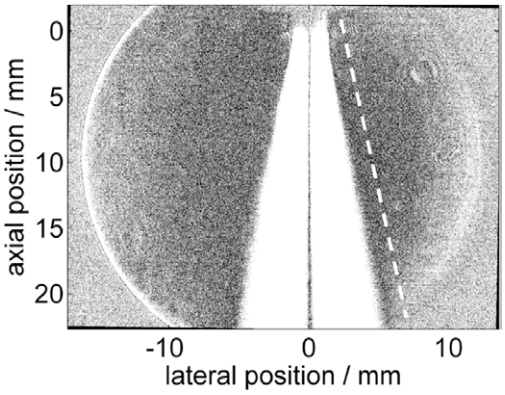

Figure 4. Displaying only contrast values close to zero makes finding the axis of symmetry easy. The dashed line indicates the upper bound that is used for the modified Abel inversion integral at the respective axial position after averaging the values from the left and right side of the axis.

2.2.4. Refractive indices. An acurate determination of the refractive indices is crucial for the correct evaluation of the Schlieren measurements. Apart from the wavelength and temperature, the refractive index of air depends on the humidity and the CO_2 content. The relative humidity in the lab was measured to be 43% using a hygrometer (DewMaster, EdgeTech, USA), the CO_2 concentration was assumed to be 450 ppm and the central transmission wavelength of the filter is 550 nm. The room temperature was measured to be 294.7 K. For the calculation of the refractive index the web application provided by the National Institute for Standards and Technology was used, which is based on the Ciddor equation and yields $n_{\mathrm{air}} - 1 = 2.713 \times 10^{-4}$ [25, 26]. For argon a refractive index $n_{\mathrm{Ar}} - 1 = 2.619 \times 10^{-4}$ for a wavelength of 546 nm was used from [27].

2.3. Computational fluid dynamics simulations

The CFD simulation was performed using COMSOL 4.2 with the CFD module as described in the previous publication [28]. The compressible Reynolds-averaged Navier–Stokes equations are solved and a standard $k - \varepsilon$-model is employed to account for the turbulence. Rotational symmetry is assumed in the model. Additionally to the simulations presented in [28], the heat transport equation

$$\rho C_p \mathbf{u} \cdot \nabla T = \nabla \cdot (k \nabla T) + Q \tag{8}$$

is coupled to the Navier–Stokes equations. Here C_p is the heat capacity at constant pressure, $\mathbf{u}$ the velocity field, k the thermal conductivity and Q is the heat source term. For the thermal conductivity the Kays–Crawford model was employed to account for the turbulent heat transport [29]. The heat capacity of the gas is weighted according to the mole fractions of argon and air as $C_p = \sum_i x_i C_{p,i}$.

The geometry used in the CFD simulation is shown in figure 6. The right hand side of figure 6 illustrates the boundary conditions used. At boundary A an inflow of 3 slm argon is defined corresponding to an average velocity $v_{\mathrm{av}} = 25$ m s^{-1} at the jet nozzle, at boundary B a normal inflow velocity of $v_B = 0.1$ m s^{-1} is defined to obtain faster convergence (further decreasing v_B does not influence the densities obtained in the effluent), at C an outlet is defined. The temperature of the inflowing gas at boundaries A and B is set to $T_0 = 294.7$ K which is the ambient room temperature measured when the Schlieren experiment was performed. All other boundaries were assumed to be thermally insulating.

Two studies corresponding to the two Schlieren experiments performed: In the first study, the heat term was set to $Q = 0$, which consequently yields an isothermal result. In the second study the heat source term was set to

$$Q = 2.36(1 - r^4/r_0^4)\ 10^8 \mathrm{W m^{-3}} \tag{9}$$

in the domain between the pin-type electrode and the nozzle exit as shown in the left part of figure 6. The total power deposited hence amounts to $P = 1.12$ W.

3. Results and discussion

3.1. Density

Figure 7 shows the mole fraction of argon obtained by the isothermal CFD simulation and the Schlieren measurement.

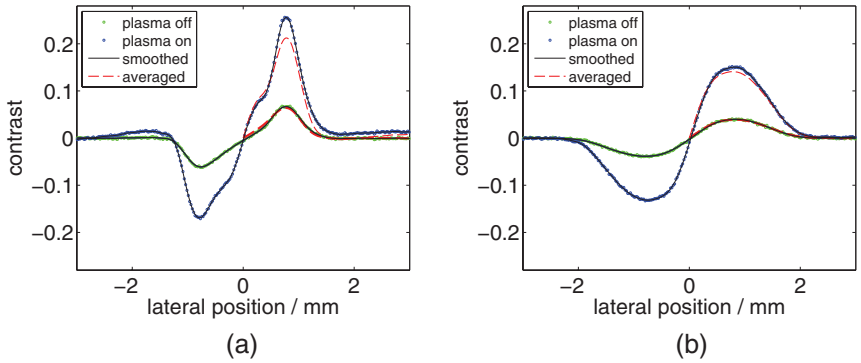

Figure 5. Lateral cuts through the data along the lines shown in figure 3 located at axial positions of (*a*) 1.5 mm and (*b*) 5 mm.

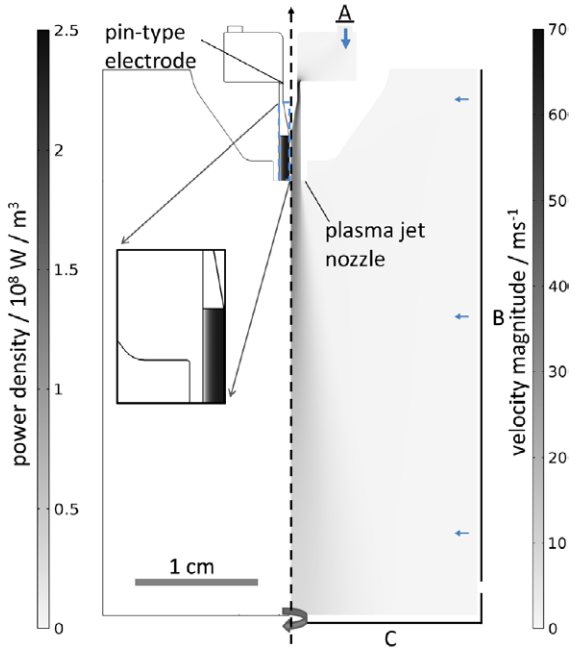

Figure 6. Geometry used in the CFD simulation. The left side illustrates the heat source term used for the thermal case, while the right side depicts the velocity magnitude and the influx of argon and air applied in the model.

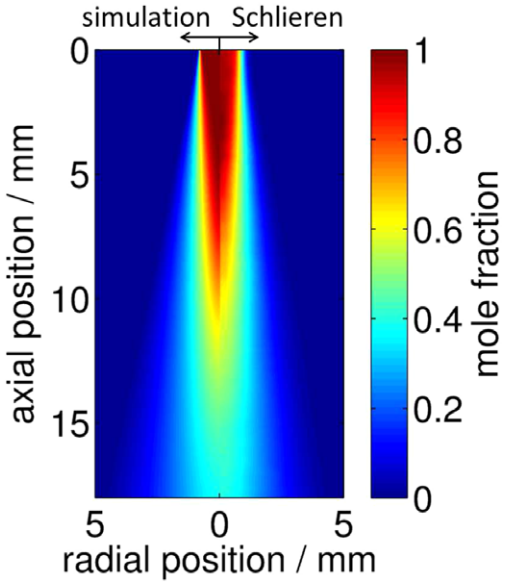

Figure 7. Mole fraction of argon obtained from CFD simulation and Schlieren measurement.

The agreement between the measurement and the simulation is very good. However, some deviations can be observed in the axial and lateral cuts of this data shown in figure 8: the on-axis density values drop a bit earlier in the measured values compared to the simulation. It is unclear however, if this is due to uncertainties in the simulations, or due to systematic errors of the measurement. The good agreement between experiment and simulation for larger radial distances ($r > 0.8$ mm) observed in figure 8(*b*) may indicate that the deviations for the on-axis values result from errors linked to the evaluation procedure: In the modified Abel inversion of the contrast values obtained for a specific radial position $r = r_1$ depend on all the data obtained in the domain $r > r_1$. Small deviations may therefore add up towards the axis. Previous CFD simulations of the jet impinging on a plate yielded very good agreement with quantitative molecular beam mass spectroscopy measurements of the on-axis densities. Another kind of deviation can be seen for the lateral cut at $z = 0.5$ mm. Here the simulated profile drops steeper than the measured profile at the rim of the nozzle. This probably results from the finite spatial resolution of the Schlieren system due to the aperture with 0.2 mm diameter. The agreement at an axial distance of 15 mm is excellent. Note that the parameter S describing the sensitivity of the Schlieren system was fitted so that we obtain an argon mole fraction of $x_{\mathrm{Ar}} = 1$ at the jet nozzle. This calibration method proved to be more accurate than the direct calculation of the sensitivity as discussed in the appendix A and also yields correct temperature values as presented in the following section.

3.2. Temperature and power

Figure 9 shows the temperature obtained by the CFD simulation with heat source and the measured temperature assuming no change in air mole fraction, hence $F = 1$ in equation (7). Compared to the mole fraction profile in figure 7 the measured temperature distribution looks very similar, which indicates that no flow regime transition occurred and, since the diffusion is dominated by the turbulent diffusive transport (the computed turbulent diffusion coefficient is 10 to 50 times larger than the molecular diffusion coefficient in the effluent region), no

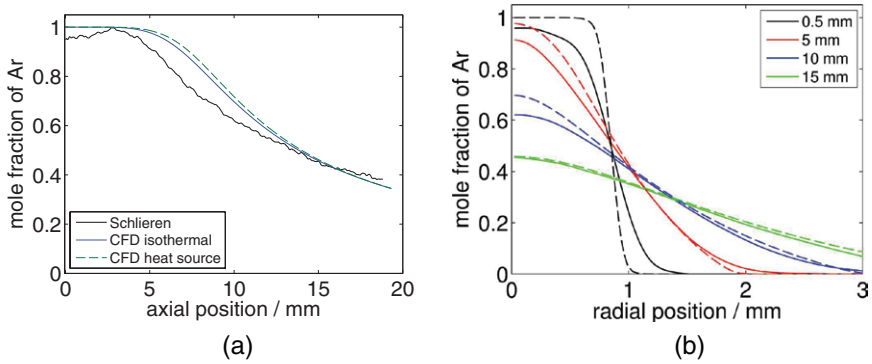

Figure 8. (*a*) Axial and (*b*) lateral cut through the density profile shown in figure 7. In (*a*) the measurement is compared to data obtained from the isothermal and thermal CFD simulation. In (*b*) the dashed lines indicate the simulation results.

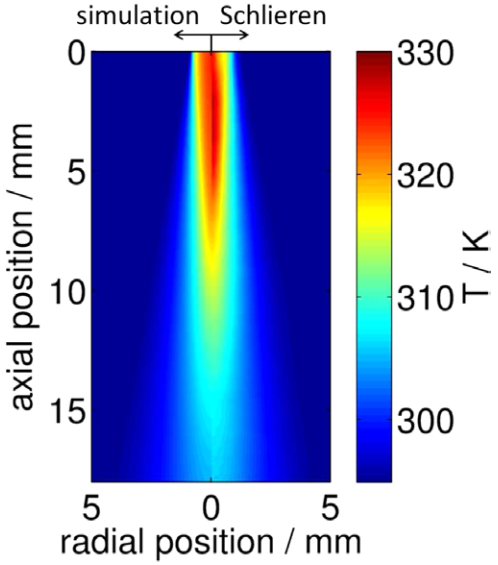

Figure 9. Temperature obtained from CFD simulation and Schlieren measurement.

drastic change in average mole fractions is expected. An absolute difference of 10% in the average mole fractions $x_{\mathrm{Ar,pl./fl.}}$ would result in a maximum error of 1.2 K according to equation (7). The experimental results are in agreement with the CFD simulations: figure 8(*a*) shows the mole fraction of argon obtained from the CFD simulations both with and without heat source and both yield almost identical mole fractions. The input power for the CFD simulation was adjusted to yield the same far-field temperature as obtained from experimental data. From experimental temperature data in figure 7 it is clear that in the near effluent some heating still occurs. In the CFD simulations this additional heat source is compensated by a broader temperature profile at the nozzle exit. This can be seen in the axial and lateral cuts presented in figure 10. Figure 10(*a*) also shows the temperature obtained from the probe measurement. Both experimental results agree very well, which was not expected a priori in the region of the visible effluent, as the probe was thought to possibly influence the plasma. However, the Schlieren measurement yields slightly higher temperature values in the region between 2 mm and 6 mm axial distance. This could result from the finite size of the temperature probe, which may lead to some slight smoothing of the temperature or from the asymmetry of the temperature field in the vicinity of the jet nozzle (see figure 5). The probe measurements also yield information about the temperature inside of the device, where the temperature appears to rise linearly from the tip of the needle electrode towards the nozzle exit. The good agreement between the experimental data and the CFD simulations in this region indicate that a quite homogeneous average volume heating inside of the device can be expected.

In figure 10(*a*) the effect of neglecting the difference between the refractive indices of argon and air also becomes clear: The uncorrected evaluation (for which $n_{\mathrm{air}} = n_{\mathrm{Ar}}$ was assumed) yields too high temperature values.

Obtaining the correct calorimetric power from the measurements requires, that not only the temperature, but also the mole fractions of argon and air are known in the far-field, as $C_{\mathrm{p,air}} \approx 2C_{\mathrm{p,Ar}}$. As evident from the far-field values shown in figures 8(*b*) and 10(*b*), both mole fractions and temperature of the CFD simulation and Schlieren measurement agree very well. As for axial distances larger than 8 mm no significant heating takes place, it can be assumed that the thermal input power of $P = 1.1$ W gives a good estimation of the thermal power deposited by the plasma jet, whereas a systematic error in the order of 5% is assumed.

The jet used in this study is very similar to the plasma jet investigated in [17], for which an ozone production rate of 2.5 10^{16} particles/s was measured. As ozone is the dominant reactive species in the far-field of the jet (the production rate of the second most abundant species NO_2 is 40 times less), this value can be used to estimate the chemical energy stored in the far-field of the jet. According to the kinetic model presented by van Gaens and Bogaerts for a similar argon CAP jet, only a small amount of atomic oxygen can be expected in the far-field (at 15 mm distance) of the jet, which is quickly converted to ozone as it reacts with molecular oxygen [30]. As ozone is almost exclusively generated from this reaction, half of the bond-dissociation energy of oxygen (497 kJ mol^{-1}) multiplied with the ozone production rate is used as an upper limit estimate for the chemical far-field power. The respective power stored in chemical energy in the far-field thus amounts to approximately 0.01 W and hence is much smaller than the thermal far-field energy. Another energy loss channel is the radiation emitted by the jet which is not quantified here but can also contain a significant part of the input power [31].

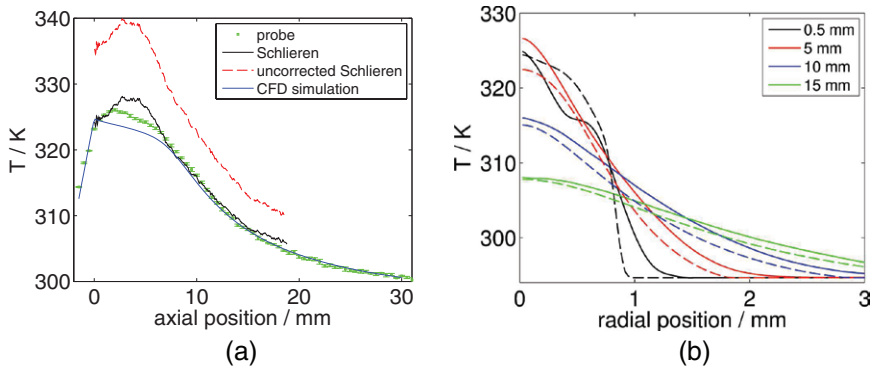

Figure 10. Axial and (*b*) lateral cut through the temperature profile shown in figure 9. In (*a*) the measurement is compared to data obtained from the CFD simulation and probe measurements. Additionally, the temperature that is obtained when the refraction of argon is not corrected for is shown. In (*b*) the dashed lines indicate the simulation results.

The thermal power value stated here is therefore a good estimate for the power that is transfered to the plasma minus the radiation losses that do not contribute to reactive species generation in the far-field. For the very similar plasma jet kinpen 09 (neoplas GmbH, Germany) a power of 1.4 W to 1.8 W was recently measured for molecular admixtures of up to 1% [32] by performing an electrical measurement following the method presented in [33]. As this method determines the total plasma input power, the slightly higher value is consistent with the value obtained in the present work.

4. Conclusion

Quantitative Schlieren measurements are a simple and precise technique for the determination of both the ambient air density and the temperature in CAP jets. The maximum temperature measured in the effluent of the CAP jet is 328 K. For obtaining precise temperature measurements it is necessary to verify that the flow regime does not change from laminar to turbulent (or vice versa) when the plasma is turned on. The fact that for low gas temperatures the change of the index of refraction due to the mixing of argon and air is in the same order of magnitude as the change due to the gas temperature is not problematic. In the contrary, the pure argon flux (with plasma turned off) can be used to calibrate the system in the sensitivity region of interest. Note, that since the jet studied operates in the turbulent flow regime and the exposure time is in the order of several seconds, the measured densities and temperatures are temporally averaged values, which on a shorter timescale undergo significant fluctuations.

The temperature obtained from the Schlieren images have been compared to measurements with an fiber-optics probe. While a deviation between both techniques was expected as the probe was thought to influence the plasma, the measured deviation was not more than 3 K. The probe was also used to measure the temperature inside of the capillary where a Schlieren measurement cannot be performed. Here a linear increase of the temperature towards the nozzle exit was found. Additionally to the measurements, CFD simulations of the jet with plasma turned off and turned on were performed. In order to mimic the heating of the gas by the exothermic reactions and thermalization of fast particles in the plasma, a heat source term was added to the heat transport equation located inside of the capillary. The simulation also yields a linear temperature increase in the capillary and produces the correct far-field air density (and hence heat capacity) and temperature. Therefore the power of 1.1 W applied in the CFD simulation gives a good calorimetric power estimation for the CAP jet. The comparison of the temperature distribution obtained from simulation and Schlieren measurement clearly shows that while most of the heat is deposited inside of the device, some heating also takes place in the effluent up to a distance of about 5 mm from the nozzle exit.

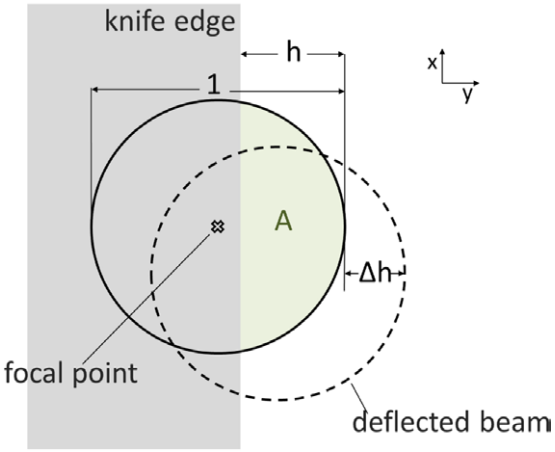

Figure A1. The aperture is imaged on the knife edge. The circle segment *A* of height is not blocked and contributes to the illumination on the CCD. A beam deflected in *y*-direction by a distance *Δ* is detected as it produces a higher or lower intensity on the CCD.

Acknowledgments

The authors would like to thank M Schöbel for his assistance in optimizing the Schlieren system. This work was supported by the German Ministry of Education and Research (BMBF, Grant No. 03Z2DN12).

Appendix A. Linear contrast region for circular apertures

Slits are more commonly used for Schlieren systems and most textbooks focus on such rectangular apertures. However,

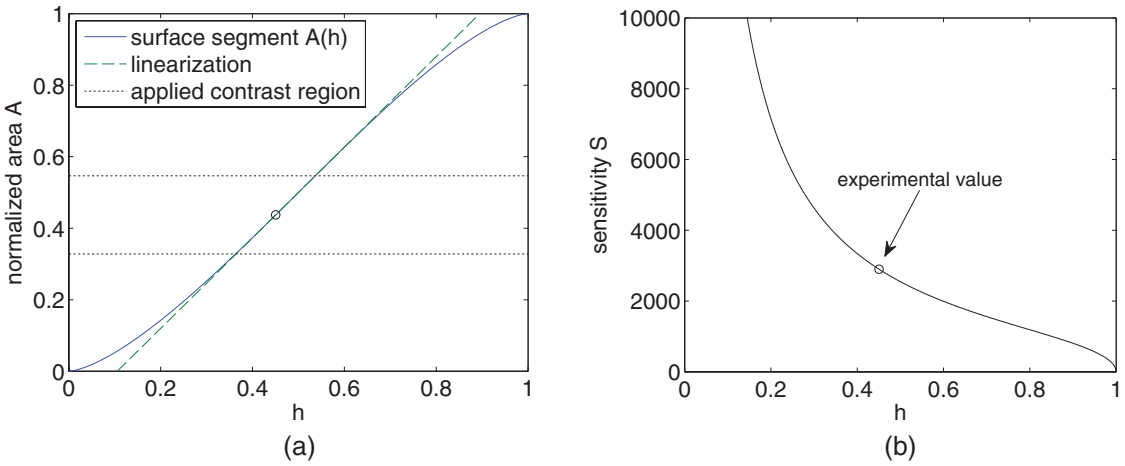

Figure A2. The circular aperture used in the Schlieren system is imaged onto the knife edge. A fraction corresponding to the normalized surface area of height h shown in (a) passes the knife edge, yielding the sensitivity as shown in (b).

circular apertures are attractive if a high spatial resolution is required. While circular apertures are covered in [4], the nonlinear behavior that can arise is neglected. In the following the issue should therefore be discussed briefly.

The Schlieren system images the aperture onto the knife edge. Let I_0 be the intensity measured on the detector without any Schlieren in the test region and without knife edge installed. When the knife edge is inserted, the intensity is homogeneously reduced to

$$I_k = I_0 A(h), \tag{A.1}$$

where

$$A(h) = (\arccos(1-2h) - 2\sqrt{h(1-h)}(1-2h))/\pi \tag{A.2}$$

is the normalized area of the segment of a circle with diameter d of height h/d as shown in figure A1(a). A beam of light that is deflected at an angle α in y-direction in the test region is hence displaced by $\Delta h = \pm \alpha f/d$ at the knife edge (for $\alpha \ll 1$), whereas the sign depends on the orientation of the knife edge. This locally leads to a change in intensity of

$$I = I_k S(h + \Delta h) \approx I_k(A(h) + \Delta h A'(h)) \tag{A.3}$$

on the detector. The contrast can now be expressed as

$$c = \frac{I - I_k}{I_k} = \frac{\Delta h A'(h)}{A(h)} = \underbrace{\pm \frac{f A'(h)}{\mathrm{d}A(h)}}_{S} \alpha \tag{A.4}$$

Together with the expression for the deviation angle (see e.g. [1] for derivation)

$$\alpha = \int \frac{\partial n}{\partial y}\, \mathrm{d}z \tag{A.5}$$

this yields equation (3) which is the basis for the quantitative evaluation of the Schlieren contrast.

The linearization in equation (A.3) is only valid if h is not too close to 0 or 1 and Δh is small. Although a higher contrast may always be achieved by choosing a lower value for h and hence increasing the factor $A'(h)/A(h)$ in (A.4), as can be seen in figure A2(a), this may result in a nonlinearity which must then be taken into account.

The sensitivity of the Schlieren system can be determined by measuring the ratio of the intensities $I_k/I_0 = A(h)$ and calculating S for the respective value of h. However, due to the strong dependence of the sensitivity on h, small errors significantly affect the densities and temperatures evaluated. For the present setup case the intensity ratio was measured to be $I_k/I_0 = 42\%$, which would yield a mole fraction of argon at the nozzle of $x_{\mathrm{Ar}} = 0.94$, which is obviously too low. The deviation is not drastic, but as the mole fraction of argon at the nozzle is known to be $x_{\mathrm{Ar}} = 1$, the system was calibrated using the argon Schlieren signal as described in section 3.1. Alternatively, the system could also be calibrated using the probe measurements for the temperature in the far-field which, as evident from figure 10, would yield the same results.

The sensitivity obtained in this way yields a value $h = 0.45$ as shown in figure A2(b), while the respective value for the circle segment is $A(h) = I_k/I_0 = 0.437$. Since the contrast in all experiments $c < 0.25$ (see figure 3) is small enough, the linearization in (A.3) can be applied.

References

[1] Goldstein R 1996 *Fluid Mechanics Measurements* (Boca Raton, FL: CRC Press)
[2] Merzkirch W 1987 *Flow Visualization* (Amsterdam: Elsevier)
[3] Settles G S 2001 *Schlieren and Shadowgraph Techniques* (Berlin: Springer)
[4] Panigrahi P K and Muralidhar K 2012 *Schlieren and Shadowgraph Methods in Heat and Mass Transfer* **2** (Berlin: Springer)
[5] Fridman G, Friedman G, Gutsol A, Shekhter A B, Vasilets V N and Fridman A 2008 Applied plasma medicine *Plasma Proc. Polym.* **5** 503–33
[6] Weltmann K D, Kindel E, von Woedtke T, Hähnel M, Stieber M and Brandenburg R 2010 Atmospheric-pressure plasma sources: prospective tools for plasma medicine *Pure Appl. Chem.* **82** 1223–37
[7] Laroussi M, Kong M G and Morfill G 2012 *Plasma Medicine: Applications of Low-Temperature Gas Plasmas in Medicine and Biology* (Cambridge: Cambridge University Press)
[8] von Woedtke T, Reuter S, Masur K and K-D Weltmann 2013 Plasmas for medicine *Phys. Rep.* **530** 291–320

[9] Jiang N, Yang J, He F and Cao Z 2011 Interplay of discharge and gas flow in atmospheric pressure plasma jets *J. Appl. Phys.* **109** 093305
[10] Oh J-S, Olabanji O T, Hale C, Mariani R, Kontis K and Bradley J W 2011 Imaging gas and plasma interactions in the surface-chemical modification of polymers using micro-plasma jets *J. Phys.* D*: Appl. Phys.* **44** 155206
[11] Ghasemi M, Olszewski P, Bradley J W and Walsh J L 2013 Interaction of multiple plasma plumes in an atmospheric pressure plasma jet array *J. Phys.* D*: Appl. Phys.* **46** 052001
[12] Robert E, Sarron V, Darny T, Riès D , Dozias S, Fontane J, Joly L and Pouvesle J-M 2014 Rare gas flow structuration in plasma jet experiments *Plasma Sources Sci. Technol.* **23** 012003
[13] Boselli M, Colombo V, Ghedini E, Gherardi M, Laurita R, Liguori A, Sanibondi P and Stancampiano A 2014 Schlieren high-speed imaging of a nanosecond pulsed atmospheric pressure non-equilibrium plasma jet *Plasma Chem. Plasma Proc.* **34** 853–69
[14] Sutton Y, Moorev J, Sharp D and Braithwaite N S J 2011 Looking into a plasma loudspeaker *IEEE Trans. Plasma Sci.* **39** 2146–7
[15] Schäfer J, Foest R, Reuter S, Kewitz T, Šperka J and K-D Weltmann 2012 Laser schlieren deflectometry for temperature analysis of filamentary non-thermal atmospheric pressure plasma *Rev. Sci. Instrum.* **83** 103506
[16] De Izarra G, Cerqueira N and De Izarra C 2011 Quantitative shadowgraphy on a laminar argon plasma jet at atmospheric pressure *J. Phys. D: Appl. Phys.* **44** 485202
[17] Schmidt-Bleker A, Winter J, Iseni S, Dünnbier M, Weltmann K D and Reuter S 2014 Reactive species output of a plasma jet with a shielding gas device: combination of ftir absorption spectroscopy and gas phase modelling *J. Phys. D: Appl. Phys.* **47** 145201
[18] Reuter S *et al* 2012 Atomic oxygen in a cold argon plasma jet: talif spectroscopy in ambient air with modelling and measurements of ambient species diffusion *Plasma Sources Sc. Technol.* **21** 24005–11
[19] Dünnbier M, Schmidt-Bleker A, Winter J, Wolfram M, Hippler R, Weltmann K D and Reuter S 2013 Ambient air particle transport into the effluent of a cold atmospheric-pressure argon plasma jet investigated by molecular beam mass spectrometry *J. Phys.* D*: Appl. Phys.* **46** 435203
[20] Foletto M, Puech V, Fontane J, Joly L and Pitchford L C 2014 Evidence of the influence of plasma jets on a helium flow into open air *IEEE Trans. Plasma Sci.* **42** 2436–7
[21] Papadopoulos P K, Vafeas P, Svarnas P, Gazeli K, Hatzikonstantinou P M, Gkelios A and Clement F 2014 Interpretation of the gas flow field modification induced by guided streamer (‘plasma bullet’) propagation *J. Phys. D: Appl. Phys.* **47** 425203
[22] Zhang S, Sobota A, van Veldhuizen E M and Bruggeman P J 2015 Gas flow characteristics of a time modulated appj: the effect of gas heating on flow dynamics *J. Phys. D: Appl. Phys.* **48** 015203
[23] Iseni S, Schmidt-Bleker A, Winter J, Weltmann K D and Reuter S 2014 Atmospheric pressure streamer follows the turbulent argon air boundary in a mhz argon plasma jet investigated by oh-tracer plif spectroscopy *J. Phys. D: Appl. Phys.* **47** 152001
[24] Garcia D 2010 Robust smoothing of gridded data in one and higher dimensions with missing values *Comput. Stat. Data Anal.* **54** 1167–78
[25] National Institute of Standards and Technology. Engineering metrology toolbox http://emtoolbox.nist.gov/Wavelength/Ciddor.asp (Last updated November 2004)
[26] Ciddor P E 1996 Refractive index of air: new equations for the visible and near infrared *Appl. Opt.* **35** 1566–73
[27] Weber M J 2002 *Handbook of Optical Materials* **19** (Boca Raton, FL: CRC press)
[28] Reuter S, Tresp H, Wende K, Hammer M U, Winter J, Masur K, Schmidt-Bleker A and Weltmann K 2012 From rons to ros: tailoring plasma jet treatment of skin cells *IEEE Trans. Plasma Sci.* **40** 2986–93
[29] Kays W M, Crawford M E and Weigand B 1980 *Convective Heat Transfer* (New York: McGraw-Hill) pp 45–57
[30] van Gaens W and Bogaerts A 2013 Kinetic modelling for an atmospheric pressure argon plasma jet in humid air *J. Phys. D: Appl. Phys.* **46** 275201
[31] Despax B, Pascal O, Gherardi N, Naude N, Belinger A and Pitchford L C 2012 Influence of electromagnetic radiation on the power balance in a radiofrequency microdischarge with a hollow needle electrode *Appl. Phys. Lett.* **101** 144104
[32] van Gaens W, Iseni S, Schmidt-Bleker A, Weltmann K-D, Reuter S and Bogaerts A 2014 Numerical analysis of the effect of nitrogen and oxygen admixtures on the chemistry of an argon plasma jet operating at atmospheric pressure *New J. Phys.* **17** 033003
[33] Hofmann S, Van Gessel A, Verreycken T and Bruggeman P 2011 Power dissipation, gas temperatures and electron densities of cold atmospheric pressure helium and argon rf plasma jets *Plasma Sources Sci. Technol.* **20** 065010